Locating the nonergodicity-parameter anomaly near the liquid-to-glass crossover temperature in $CaKNO_3$ by Brillouin scattering

G. Li, W. M. Du, J. Hernandez, and H. Z. Cummins
Department of Physics, City College of the City University of New York, New York, New York 10031
(Received 19 January 1993)

A Brillouin-scattering experiment was performed on the ionic glass former $CaKNO_3$ to determine the temperature dependence of the nonergodicity parameter $f(T)$ of mode-coupling theory. The spectra were analyzed using a generalized hydrodynamics formulation with most of the parameters fixed by previously reported experimental results. A conventional Cole-Davidson model for the memory function was found to be inadequate due to the neglect of β relaxation. An empirical memory function including both α and β relaxation was therefore constructed, based on a previous depolarized-light-scattering study. It was found to provide good fits to the spectra for the whole temperature range studied. The resulting nonergodicity parameter exhibits a cusp anomaly as predicted by mode coupling theory at $T \sim 102\,^{\circ}\mathrm{C}$, in good agreement with the crossover temperature T_c found from previous neutron-scattering and depolarized-light-scattering studies. Our results also suggest that fits of data for supercooled liquids to phenomenological α-relaxation-only models may generally tend to underestimate the relaxation time.

PACS number(s): 64.70.Pf, 78.35.+c, 83.50.Fc

I. INTRODUCTION

When a liquid is cooled below its bulk melting temperature T_m, crystallization usually begins rapidly. For materials with sufficient anisotropy or complexity to frustrate nucleation, however, if the temperature is lowered fast enough the liquid can be supercooled indefinitely until all liquidlike properties disappear and it then responds to external probes as an amorphous solid or glass. In the supercooled-liquid region between T_m and the glass-transition temperature T_g (usually defined as the temperature at which the viscosity reaches 10^{13} P), the viscosity η and the characteristic relaxation time τ increase by at least 14 orders of magnitude.

The resulting viscoelastic behavior of supercooled liquids approaching the liquid-glass transition has been investigated extensively by many different techniques for over 100 years. But the origin of this strongly temperature-dependent slow-relaxation behavior, and its relation to the glass transition itself, remains unresolved. Since the pioneering work of Maxwell, it has been customary to represent structural relaxation by simple parametrized phenomenological functions, and to determine the parameters by fitting to experimental data.

Recently, a new theoretical approach to supercooled-liquid dynamics and the liquid-glass transition known as the mode-coupling theory (MCT) has been developed in which structural relaxation results from retarded nonlinear interactions among density-fluctuation modes (for recent reviews, see Refs. [1] and [2]). MCT provides detailed predictions for many experimentally accessible aspects of the liquid-glass-transition dynamics and has motivated many of the recent experimental investigations of the liquid-glass transition.

A central prediction of the MCT in its original idealized form is the occurrence of an ergodic-to-nonergodic transition at a crossover temperature T_c where the nonlinear interactions, which become stronger with decreasing temperature, induce a structural arrest with several characteristics of experimentally observed liquid-glass transitions. For any given material, MCT predicts that anomalies occur at T_c for all variables that couple to density fluctuations [3]. Therefore, the same T_c should be found for a given material from *any* appropriate experiment, e.g., neutron scattering, light scattering, ultrasonics, etc. In particular, it should show up in the dynamic structure factor $S(q,\omega)$ no matter whether one chooses a small wave vector q as in light scattering or a large q as in neutron scattering.

The idealized MCT also predicts that for T above but close to T_c, the normalized correlation function of a density-fluctuation mode will relax (following an initial microscopic phononlike transient) via a two-step process: an initial power-law critical decay towards a plateau f, followed by a second power-law decay which is the beginning of the primary α-relaxation process. This α process, which determines the viscoelastic relaxation time, is the usual relaxation observed in most experiments and represented by phenomenolgical models. The faster β-relaxation process, which preceeds it in time, occurs in the relaxation spectrum at higher frequencies above the α-relaxation peak and is not easily observed. As $T \to T_c+$, the critical decay region extends to longer and longer times until, at $T = T_c$, the α-relaxation process arrests. The correlation function then develops a $t \to \infty$ aymptotic value of f, designated as the nonergodicity parameter or Debye-Waller factor. As T is further decreased, $f(T)$ is predicted to increase as $\sqrt{T_c - T}$.

The principle experimental evidence supporting MCT came from neutron-scattering observations of this predicted square-root cusp in $f(T)$. Mezei, Knaak, and Farago [4] estimated T_c for $CaKNO_3$ (CKN, an ionic glass

former) $\sim 35\,^{\circ}$C above the calorimetric glass-transition temperature $T_g \approx 60\,^{\circ}$C; Frick, Farago, and Richter [5] found T_c for polybutadiene (a polymer glass former) $\sim 35\,^{\circ}$C above T_g; Börjesson, Elmroth, and Torell [6] found T_c for propylene carbonate (PC, a molecular glass former) $\sim 50\,^{\circ}$ above T_g; and Petry *et al.* [7] reported a wave-vector-independent T_c for orthoterphenyl (also a molecular glass former) $\sim 50\,^{\circ}$ above T_g. Recently, we have reported depolarized-light-scattering studies of CKN [8] and Salol [9] (another molecular glass former) which gave $T_c \approx T_g + 45\,^{\circ}$C and $T_c \approx T_g + 38\,^{\circ}$C, respectively. The agreement of our CKN result with the neutron result [4] supports the MCT prediction that T_c should be independent of the specific experimental technique employed.

Fuchs, Götze, and Latz [10] pointed out that for long-wavelength density-fluctuation modes, $f(T)$ could be determined from the high- and low-frequency sound velocities measured in ultrasonic or Brillouin-scattering experiments, opening the way for a test of the theory in a previously inaccessible wave-vector region. The first experiment to pursue this approach was a Brillouin-scattering study of PC by Elmoth, Börjesson, and Torell [11] who employed a generalized hydrodynamics approach with a Cole-Davidson (CD) function for the relaxing memory function. Their data analysis revealed a square-root cusp in $f(T)$ at 270 K, implying a value of T_c at least $60\,^{\circ}$C higher than the neutron-scattering result [6, 12] (and $50\,^{\circ}$C above the melting temperature T_m), challenging the applicability of the MCT as an appropriate description of supercooled-liquid dynamics. A subsequent study of Salol [13], which combined Brillouin-scattering and ultrasonic measurements, also modeled the structural relaxation by a CD function, and found that $T_c \approx T_g + 57\,^{\circ}$C, in reasonable agreement with, but slightly higher than, the result of the depolarized light-scattering study [9].

Götze [14] suggested that discrepancies between the T_c values obtained from neutron-scattering experiments and Brillouin-scattering experiments may result in part from ignoring the β-relaxation contribution to the memory function. Indeed, as can be seen clearly in the depolarized-light-scattering spectra in Refs. [8, 9], for temperatures near T_c the Brillouin components are within the β-relaxation region, which suggests that an analysis based on α-relaxation-only models is likely to produce unreliable results.

To explore the importance of β relaxation in the determination of T_c by this method, we have undertaken another Brillouin-scattering study of CKN. As we shall show, an analysis using the CD memory function is clearly inadequate for CKN. We have therefore developed an alternative approach in which an empirical memory function is reconstructed from the depolarized-light-scattering spectra. This procedure, which takes full account of β-relaxation effects, leads to a consistent interpretation of the Brillouin spectra and results in a value of T_c in good agreement with values determined by other methods. Our analysis shows that data analysis based on α-relaxation-only memory-function models tends to produce artificial values for the structural relaxation time τ which are smaller than values determined by direct measurement.

In Sec. II we briefly review the mode-coupling theory, the generalized hydrodynamics approach to interpreting Brillouin-scattering spectra, and the determination of $f(T)$ and T_c from Brillouin spectra. The experiment and experimental results are described in Sec. III, with details of the analysis given in Sec. IV. In Sec. V we briefly describe an alternative experimental approach to finding $f(T)$ and T_c from Brillouin-scattering spectra. Our summary and conclusions are presented in Sec. VI.

II. THEORY

A. Mode-coupling theory and the nonergodicity parameter

The mode-coupling theory of the liquid-glass transition is primarily concerned with the normalized density correlation function

$$\Phi_q(t) = \langle \delta\rho_q(0)\delta\rho_q^*(t)\rangle / S_q \ , \tag{2.1}$$

where $\delta\rho_q$ is the time-dependent qth Fourier component of the density fluctuation $\delta\rho$ and $S_q = \langle|\delta\rho_q(0)|^2\rangle$ is the static structure factor. $\Phi_q(t)$ can be shown to obey the equation of motion

$$\ddot{\Phi}_q(t) + \gamma_q\Omega_q^2\dot{\Phi}_q + \Omega_q^2\Phi_q(t) + \Omega_q^2\int_0^t dt' m_q(t-t')\dot{\Phi}_q(t') = 0 \ , \tag{2.2}$$

where γ_q is a regular damping constant, Ω_q is the microscopic frequency, and $m_q(t)$ is the memory function. Within the idealized MCT, which does not include activated hopping processes, the memory function (or kernel) is expressed as

$$m_q(t) = \sum_{q_1} V^{(1)}(q,q_1)\Phi_{q_1}(t) + \sum_{q_1,q_2} V^{(2)}(q,q_1,q_2)\Phi_{q_1}(t)\Phi_{q_2}(t) + \cdots \ , \tag{2.3}$$

where the $V^{(i)}$ are coupling constants which can be expressed in terms of the static structure factor S_q [15]. Complete self-consistent solutions of Eqs. (2.2) and (2.3) can be obtained by restricting both the range of q values and the number of coupling coefficients. Solutions to these schematic models exhibit the general behavior illustrated in Fig. 1 for the F_{12} model [1]. As the strength of the coupling constant $V^{(1)}$ increases (with $V^{(2)} = 2.0$), structural arrest occurs at $V^{(1)} = 0.8284$, and the nonergodicity parameter $f_q(T)$ [the $t \to \infty$ intercept of $\Phi_q(t)$] increases discontinuously from 0 to f_q^c. Since in a neutron-scattering experiment a nonzero $\Phi_q(t \to \infty)$ would produce elastic scattering, $f_q(T)$ is also called the Debye-Waller factor.

In practice, neutron-scattering experiments do not measure elastic scattering, but instead determine the integrated intensity of the quasielastic line within some

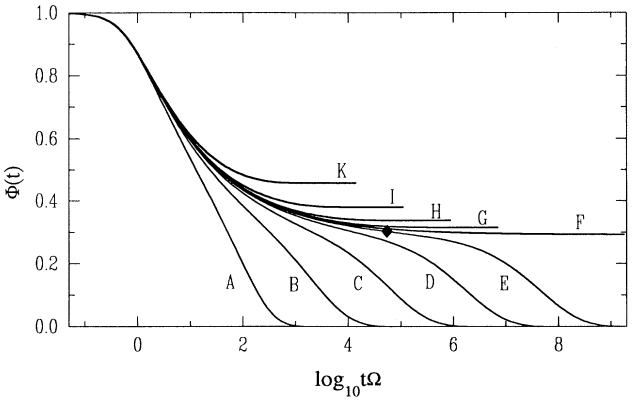

FIG. 1. $\Phi_q(t)$ vs $\log_{10}(t\Omega_q)$ from the MCT schematic F_{12} model [1] with $m_q(t) = V^{(1)}\Phi_q(t) + V^{(2)}\Phi_q^2(t)$ in Eq. (2.2). $\gamma_q = 5$, $V^{(2)} = 2.0$, $V^{(1)} = 0.8284 \pm 0.4/2^n$. Liquid (−): $n = 0$ (A), 2 (B), 4 (C), 6 (D), 8 (E); critical correlator (F); glass (+): $n = 8$ (G), 6 (H), 4 (I), 2 (K). (Computed by M. Fuchs.) For (F) through (I) the $t \to \infty$ intercept is the nonergodicity parameter $f(T)$. The diamond on (E) indicates the "plateau" corresponding approximately to the effective nonergodicity parameter of Eq. (2.4).

narrow energy window ΔE. $f_q(T)$ therefore corresponds to the value $\Phi_q(t)$ at a finite time $t = h/(2\pi\Delta E)$. The effective nonergodicity parameter $f_q(T)$ is then predicted to obey

$$f_q(T) = f_q^c + \begin{cases} h_q\sqrt{\sigma} + O(\sigma) , & T < T_c \\ O(\sigma) , & T > T_c \end{cases} \tag{2.4}$$

where $\sigma \propto (T_c - T)/T_c$ is the separation parameter. For $T > T_c$, $f_q(T)$ which is the area under the quasielastic line (presumed to include only the α peak) varies smoothly with temperature, but for $T < T_c$ it varies critically following a $\sqrt{\sigma}$ law, i.e., T_c is marked by a square-root cusp [16]. [MCT predicts that T_c should show up as a cusp in $f_q(T)$ for small q at the same T as for large q.] If the two time scales for decay of $\Phi_q(t)$ are well separated, $f_q(T)$ represents the initial plateau value at the onset of α relaxation for $T > T_c$. When activated hopping effects are included, the extended MCT predicts restoring of ergodicity below T_c. Since in the extended theory, $\Phi_q(t \to \infty) = 0$ even for $T < T_c$, an effective nonergodicity parameter $\tilde{f}(T)$ was defined as the value of $\Phi_q(t)$ at the inflection point, the long-time limit of the critical relaxation, and the short-time limit of the α relaxation [17]. With this definition the effective nonergodicity parameter essentially follows the same behavior as Eq. (2.4) but some smearing out of the cusp may occur due to hopping effects [18].

B. Generalized hydrodynamic equations for Brillouin scattering

Polarized Brillouin-scattering spectra primarily determine $S(q,\omega)$ of small-q longitudinal density fluctuations $\delta\rho_q(t)$. A theoretical expression for $S(q,\omega)$ can be derived from the linearized equations of hydrodynamics both for simple fluids [19] and fluids exhibiting relaxation effects [20], following the procedure described by Mountain.

A simplified version of Mountain's approach can be used if the very-low-frequency spectral region, which contains the noncritical thermal diffusion mode (Rayleigh line) is ignored. This approach, and its relation to Mountain's equations, was discussed by Montrose, Solovyev, and Litovitz [21] and by Tao, Li, and Cummins [22]. It leads to an equation of motion for $\Phi(t) = [\Phi_q(t)]_{q\to 0}$,

$$\ddot{\Phi}(t) + \gamma\dot{\Phi}(t) + \omega_0^2\Phi(t) + \int_0^t dt' m(t-t')\dot{\Phi}(t') = 0 . \tag{2.5}$$

With the Laplace transform convention

$$\mathcal{L}[f(t)] = i\int_0^\infty \exp(izt)f(t)dt = f(z) , \tag{2.6}$$

the normalized spectrum

$$S(q,\omega)/S(q) = (1/\pi)\mathrm{Im}[\Phi(z)]_{z=\omega}$$

becomes

$$\frac{S(q,\omega)}{S(q)} = \frac{[\gamma + m''(\omega)]\omega_0^2/\pi}{[\omega^2 - \omega_0^2 + \omega m'(\omega)]^2 + \{\omega[\gamma + m''(\omega)]\}^2} , \tag{2.7}$$

where $\omega_0 = C_0 q$ is the adiabatic sound velocity and γ is the damping constant. (In practice, ω_0 and γ will be determined experimentally.)

Note that Eq. (2.5) has the same structure as the MCT equation (2.2) (except for different conventions for factorization by Ω_q^2 or ω_0^2 in the second and fourth terms) so that, in principle, the $q \to 0$ memory function $m(t)$, expressed in terms of the appropriate coupling constants $V^{(i)}$, could be calculated within MCT.

C. Determining $f(T)$ and T_c from Brillouin spectra

1. Debye relaxation

The simplest approximation for the memory function $m(t)$ of Eq. (2.5) is the Debye single-relaxation approximation $m(t) = \Delta^2 e^{-t/\tau}$ or $m(z) = i\Delta^2\tau/(1 - iz\tau)$, which leads to the following well-known results. (i) The Brillouin peak occurs at $\omega_B = \omega_0$ if $\omega_0\tau \ll 1$, and at $\omega_B = \sqrt{\omega_0^2 + \Delta^2} \equiv \omega_\infty$ if $\omega_0\tau \gg 1$. (ii) The Brillouin linewidth is a maximum (as a function of τ) at $\omega_B\tau = 1$. A third result, noted by Mountain [20], follows from the complex form of Eq. (2.7) with the Debye $m(z)$, when the denominator is factored to $(z-z_1)(z-z_2)(z-z_3)$. If the three roots are well separated, then the central peak (the "Mountain mode") is a narrow Lorentzian function of integrated intensity $\Delta^2/(\omega_0^2 + \Delta^2)$.

Since the central peak intensity is just $f(T)$ of the MCT [the long-wavelength ($q \to 0$) limit of $f_q(T)$], by identifying $\omega_0 = C_0 q$ and $\omega_\infty = C_\infty q$ we obtain the result of Fuchs, Götze, and Latz [10],

$$f(T) = 1 - \frac{\omega_0^2}{\omega_\infty^2} = 1 - \frac{C_0^2}{C_\infty^2}, \tag{2.8}$$

where C_0 and C_∞ correspond, respectively, to the sound velocity measured below and above the α relaxation. Actually, Eq. (2.8) is far more general than the particular choice of the Debye form for $m(t)$. It can be shown that *any* spectral shape for the central peak gives the same result, as long as it is sufficiently narrow to be clearly separated from the Brillouin peaks. This requires that $\omega_0^2 - \omega m'(\omega)$ in Eq. (2.7) should increase from ω_0^2 at low frequencies to a "plateau" $\omega_0^2 + \Delta^2$ at high frequencies where $\omega m''(\omega)$ is zero. As previously pointed out by Fuchs, Götze, and Latz [10], if no such plateau exists, then ω_∞ is not well defined, and Eq. (2.8) cannot reliably determine $f(T)$.

2. *Kohlrausch and Cole-Davidson models*

Since experimental evidence indicates that relaxation processes in supercooled liquids are generally stretched, more realistic α-relaxation models than the Debye model are usually used, such as the stretched exponential (Kohlrausch) function

$$m(t) = \Delta^2 \exp[-(t/\tau)^\beta] , \tag{2.9}$$

which was used, e.g., for analyzing CKN Brillouin data [23] or the CD function

$$\omega m(\omega) = \Delta^2[(1 - i\omega\tau_{\rm CD})^{-\beta_{\rm CD}} - 1] , \tag{2.10}$$

which was employed in the analysis of Brillouin data for PC [6] and Salol [13]. (Approximate relations between the CD coefficients $\tau_{\rm CD}$ and $\beta_{\rm CD}$ and the Kohlrausch coefficients τ and β have been determined by Lindsey and Patterson [24].)

The position of the Brillouin peaks ω_B in Eq. (2.7) is given, to a good approximation, by the roots of $\omega^2 - \omega_0^2 + \omega m'(\omega) = 0$. For the models of Eqs. (2.9) and (2.10), just as for the Debye model, one finds that for $\omega_0\tau$ (or $\omega_0\tau_{\rm CD}$) $\ll 1$

$$\omega_B^2 = \omega_0^2 , \quad C_B^2 = C_0^2 , \tag{2.11}$$

while for $\omega_0\tau$ (or $\omega_0\tau_{\rm CD}$) $\gg 1$,

$$\omega_B^2 = \omega_0^2 + \Delta^2 = \omega_\infty^2 , \quad C_B^2 = C_0^2 + (\Delta/q)^2 = C_\infty^2 , \tag{2.12}$$

where $C_B = \omega_B q$. Therefore, by fitting experimental Brillouin spectra to Eq. (2.7) with the memory-function model of Eq. (2.9) or (2.10), one can in principle obtain ω_0 and Δ which will provide C_0 and C_∞, and thus determine $f(T)$ via Eq. (2.8).

This procedure is far from straightforward, however, because the frequency range available in the Brillouin-scattering experiment is typically just over one decade, while the relaxation function covers many decades. As noted 25 years ago by Montrose, Solovyev, and Litovitz [21], for liquids exhibiting a distribution of relaxation times, extracting useful information from such fits is hampered by the fact that the experimental data can often provide acceptable fits within a rather wide variation of the adjustable parameters. More recently, Fuchs, Götze, and Latz [10] have reached similar conclusions in reanalyzing previously published Brillouin-scattering data where they found that the analysis was unstable with parameter variations, particularly for the temperature dependence of the stretching coefficient β. It seems clear that in order to deduce meaningful results from such fits, it is necessary to draw on independent characterization of the relaxation function, reducing the number of fitting parameters to a minimum. This problem is further exacerbated if one also attempts to include β relaxation which is not taken into account in these conventional models.

3. *Empirical memory function*

Previous Brillouin-scattering studies of the liquid-glass transition have all been analyzed with models for the memory function $m(\omega)$ which contain only the α relaxation, such as the single- or stretched-exponential relaxation model Eq. (2.9) or the CD function Eq. (2.10). However, neutron-scattering [25–27] and light-scattering [28, 8, 9] experiments have demonstrated the existence of intermediate-frequency β relaxation located between the low-frequency α relaxation and the high-frequency microscopic excitation band as predicted by the MCT, which may influence the spectrum of Eq. (2.7).

Figure 2, from Ref. [8], shows CKN depolarized-light-scattering spectra $I_{\rm VH}(\omega)$ (a) and corresponding susceptibility spectra $\chi''(\omega)$ (b) [a small longitudinal-acoustic (LA) leakage signal appears at $\sim$ 20 GHz.] It can be seen that the α-relaxation peak in $\chi''(\omega)$ moves rapidly to lower frequencies with decreasing temperature, and disappears from the spectral window (0.3–10^4 GHz) by

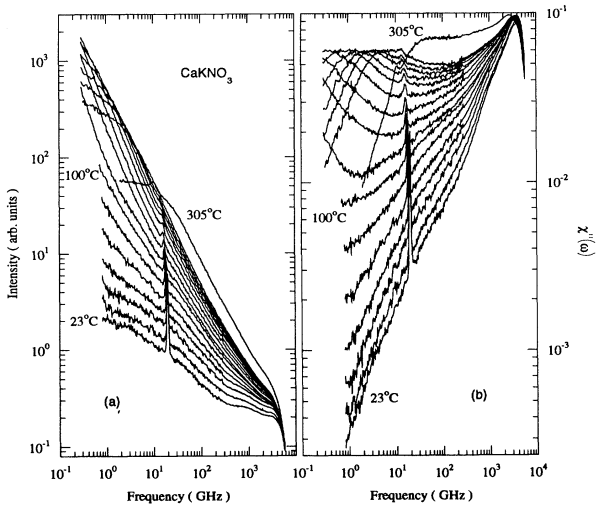

FIG. 2. CKN depolarized $\theta = 173°$ light-scattering spectra $I_{\rm VH}(\omega)$ (a) and susceptibility spectra $\chi''(\omega) = I_{\rm VH}(\omega)/[n(\omega) + 1]$ (b) obtained from depolarized-light-scattering spectra [8]. Note that for temperatures below 130 °C the frequency of the (leakage) LA mode is above the position of the susceptibility minimum, and is therefore in the critical-decay part of the β-relaxation region to the left of the plateau in Fig. 1.

$T \approx 120\,^{\circ}\mathrm{C}$. For $T < 140\,^{\circ}\mathrm{C}$ the Brillouin peak is located in the β-relaxation region at a frequency well above the susceptibility minimum [which corresponds approximately to the time at which $\Phi(t)$ crosses the plateau]. In this situation, as we shall show below, the β-relaxation contribution causes the Brillouin peak to occur at a frequency *above* ω_∞ due to the α relaxation, so Eq. (2.8) will give too large a result for f if ω_B is assumed to be ω_∞.

The depolarized-light-scattering spectra of Fig. 2(a), $I_{\mathrm{VH}}(\omega) = R'(\omega)$, are related to $R(t)$, the correlation function of the scattered optical field $E_s(t)$ by the Wiener-Khintchine relation,

$$I_{\mathrm{VH}}(\omega) = R'(\omega) = (1/\pi)\mathrm{Re}\int_0^\infty R(t)e^{i\omega t}dt\ . \quad (2.13)$$

From $R'(\omega)$, one can find $R''(\omega)$ by a Kramers-Kronig (KK) transform to complete the complex function $R(\omega) = R'(\omega) + iR''(\omega)$.

We now postulate that for CKN the complex function $R(\omega)$ is proportional to the complex memory function $m(\omega)$. Noting the difference between the Fourier transform convention Eq. (2.13) and the Laplace transform convention Eq. (2.6) for $m(\omega)$, we take $m(\omega) = m'(\omega) + im''(\omega)$, where

$$\begin{aligned} m'(\omega) &= -BR''(\omega)\ , \\ m''(\omega) &= BR'(\omega)\ , \end{aligned} \quad (2.14)$$

where B is an unknown proportionality constant. Thus $m''(\omega)$ will be determined directly (apart from the constant B) from the $I_{\mathrm{VH}}(\omega)$ spectra of Fig. 2(a), and $m'(\omega)$ will be found from $m''(\omega)$ by the KK transformation:

$$m'(\omega) = \frac{2\omega}{\pi}\int_0^\infty \frac{m''(\omega) - m''(x)}{\omega^2 - x^2}dx\ . \quad (2.15)$$

To justify this ansatz, we note that the scattered light signal, represented by $R(t)$ in Eq. (2.13), arises primarily from second- (or higher-) order dipole-induced-dipole (DID) scattering processes plus some orientational fluctuations of the anisotropic NO_3 ions. In the β-relaxation region, the MCT predicts a universal β-correlation function for all dynamical variables of the supercooled liquid. Thus, in the β regime (which includes the high-frequency wing of the α peak), the ansatz of Eq. (2.14) is fully justified by MCT.

To justify its extension to the α-relaxation regime, we have previously proposed that $R(t)$ is dominated by second-order scattering from pairs of density-fluctuation modes near q_0, the first peak of the static structure factor $S(q)$, so that $R(t) \propto \phi^2_{q_0}(t)$ which is also the dominant term in Eq. (2.3). We have tested this relation for CKN by comparing the α peaks of the depolarized light-scattering spectra with the results of neutron spin-echo experiments which determine $\phi_{q_0}(t)$ directly (Ref. [8], Fig. 15). Also, the identification of $R(\omega)$ with $m(\omega)$ is supported for CKN by the fact that the Brillouin linewidth γ_B of the LA mode shows a maximum at $T \approx 230\,^{\circ}\mathrm{C}$ [24] (see Fig. 5) where the α peak of the $\chi''(\omega)$ curve ω_α [8] crosses the frequency of the LA mode ω_B (see Fig. 2). Such a coincidence is expected from Eq. (2.7) if Eq. (2.14) is valid.

III. EXPERIMENTAL METHODS AND RESULTS

The CKN sample used in this experiment was prepared from Alfa products KNO_3 (99.999%) and $Ca(NO_3)_2{\cdot}4HO_2$ (99.9995%). The detailed sample preparation procedure has been described in Ref. [8]. No crystallization occured in the sample during the experiments.

Brillouin-scattering measurements were performed in the temperature range from 341 to $-197\,^{\circ}\mathrm{C}$. The cooling rate between runs was $\sim 0.5\,^{\circ}\mathrm{C/min}$. For the measurements above room temperature, the CKN sample, contained in a glass tube of diameter $\sim$ 1.5 cm, was placed in an Oxford high-temperature furnace [8]. For low-temperature measurements, the sample, contained in a glass cell of $\sim$ 1.5 cm in both height and diameter, was installed in an Oxford ND1754 cryostat, with the temperature controlled by an Oxford ITC4 temperature controller. Although the solidified sample cracked at low temperatures, we were always able to find a clear crack-free region for the measurements.

Our Brillouin-scattering spectrometer is based on a six-pass (3+3) Sandercock tandem Fabry-Pérot interferometer which has also been described in a previous publication [33]. To avoid the influence of Brillouin scattering from transverse-acoustic modes in the low-temperature measurements, we selected a large-angle ($\theta = 173^{\circ}$) scattering geometry. The mirror separation used was $d = 0.5$ cm. The Spectra Physics model 165 argon-ion laser was operated at 4880 Å with a typical power of $\sim$ 30 mW. A typical collection time for each spectrum was $\sim$ 15 min.

To study the dynamics of the longitudinal sound wave which is associated with the density fluctuation $\delta\rho_q(\omega)$, it is important to obtain Brillouin spectra which contain only the contribution from the LA mode. The vertical-vertical (VV) Brillouin spectrum of a liquid contains not only the contribution from the first-order scattering of the LA mode, but also the anisotropic-scattering contributions from molecular orientational motion and second- (and higher-) order DID scattering.

To eliminate the anisotropic-scattering contributions, we first measured the depolarization ratio in the frequency range of 40 to 260 GHz, which is far outside the LA-mode Brillouin range. Presumably, the VV and vertical-horizonal (VH) spectra in this frequency range both come predominantly from the anisotropic contributions. Using a mirror separation of $d = 0.5$ mm and a scattering angle of $\theta = 173^{\circ}$, we obtained VV and VH spectra at temperatures $T = 341$, 122, and $45\,^{\circ}\mathrm{C}$. Figure 3(a) displays the VV spectrum for $122\,^{\circ}\mathrm{C}$, and Fig. 3(b) shows the corresponding inverse depolarization ratio $I_{\mathrm{VV}}(\omega)/I_{\mathrm{VH}}(\omega)$. We found $I_{\mathrm{VV}}(\omega)/I_{\mathrm{VH}}(\omega) = 1.28$. (With correction for the instrumental polarization dependence, the depolarization ratio is $I_{\mathrm{VH}}/I_{\mathrm{VV}} \cong 0.64$.) The same result was obtained for $T = 341$ and $45\,^{\circ}\mathrm{C}$, suggesting that the depolarization ratio is frequency and temperature independent. Assuming that this result is also true for lower frequencies, we can then identify the

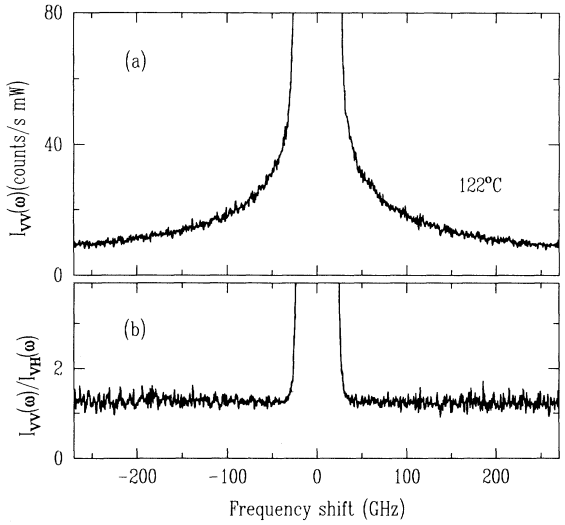

FIG. 3. (a) VV Brillouin spectrum ($\theta = 173°$) of CKN at $T = 122\,°C$; (b) the corresponding ratio $I_{VV}(\omega)/I_{VH}(\omega)$. A frequency-independent ratio $I_{VV}(\omega)/I_{VH}(\omega) = 1.28$ was found for $T = 341$, 122, and 45 °C. (With the correction for instrumental polarization dependence, the depolarization ratio is $I_{VH}/I_{VV} = 0.64$.)

contribution of anisotropic scattering to a normal VV Brillouin spectrum in the LA-mode frequency range by using the corresponding VH spectrum multiplied by 1.28.

Figure 4 shows a comparison of these contributions at $T = 211\,°C$. The upper spectrum in Fig. 4(a) is the experimental VV Brillouin spectrum; the lower spectrum, shows only a central peak, is the VH spectrum. By subtracting $1.28I_{VH}(\omega)$ from $I_{VV}(\omega)$, we obtain the corrected VV spectrum shown in Fig. 4(b) which, presumably, is the pure isotropic Brillouin spectrum of the LA mode, $I_{LA}(\omega)$. Comparing the VV spectrum in Fig. 4(a) and the corrected LA spectrum in Fig. 4(b), one can see that almost half of the central-peak intensity in the experimental VV spectrum (a) comes from the anisotropic contribution, which seriously affects the spectral shape. Therefore we conclude that the anisotropic contribution to the VV Brillouin spectrum is important for CKN and must be taken into account before performing the theoretical fits. (A similar result was found for Salol [13].)

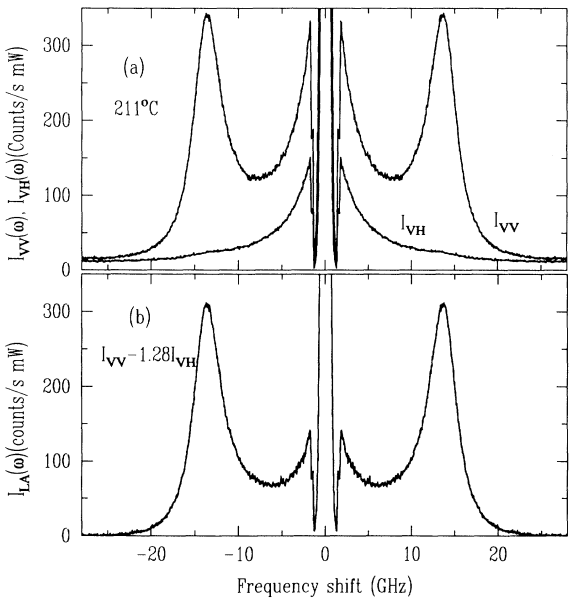

FIG. 4. (a) VV and VH Brillouin spectra ($\theta = 173°$) of CKN at $T = 211\,°C$. (b) Pure LA-mode Brillouin spectrum $I_{LA}(\omega) = I_{VV}(\omega) - 1.28I_{VH}(\omega)$.

Following the procedure illustrated in Fig. 4, we then obtained a set of pure LA-mode Brillouin spectra $I_{LA}(\omega)$ for different temperatures. In obtaining $I_{VV}(\omega)$ and $I_{VH}(\omega)$ spectra, the background due to dark counts and stray light has been eliminated by using reference spectra collected with the reference beam of the laser as the only input signal. Therefore the corrected $I_{LA}(\omega)$ spectra do not contain a background.

Note that in Refs. [23, 13], the anisotropic contribution has also been taken into account in the Brillouin-scattering studies of CKN and Salol, but the amplitude was treated as an additional adjustable parameter in the analyses. With $I_{LA}(\omega)$ spectra obtained by the procedure shown in Fig. 4, this parameter is eliminated.

In Fig. 5, we show the temperature dependence of the Brillouin-peak frequency ω_B (circles) and the damping constant γ_B (full width of the Brillouin peaks at half maximum, squares) obtained by fitting the main Brillouin peaks of the $I_{LA}(\omega)$ spectra with the imaginary part of a damped-harmonic-oscillator response function multiplied by a Bose factor and convoluted with the instrumental function. (These ω_B and γ_B values are also listed in Table I.) The solid line in Fig. 5 is $\omega_0 = C_0 q$ calculated from published ultrasonic results [29,32]: $C_0(\mathrm{cm/s}) = 2.01\times10^5 - 83.33T$ (°C), and a linear fit to refractive index data: $n(T) = 1.51 - 1.60 \times 10^{-4}T$

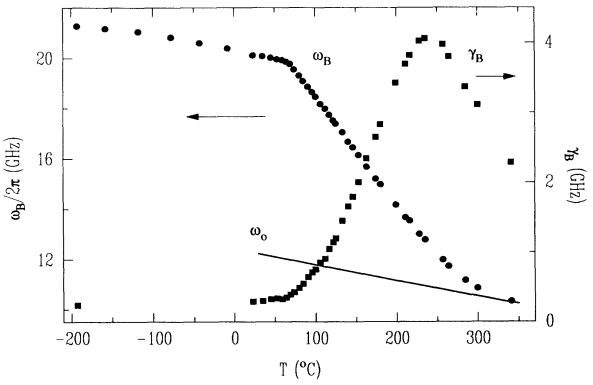

FIG. 5. Temperature dependence of the LA-mode Brillouin frequency ω_B (circles) and the damping constant γ_B (squares) of CKN obtained from 173 ° scattering. The value of ω_0 (solid line) was calculated from extrapolated ultrasonic results [29, 32] and refractive index measurements [30].

(°C) [30]. Note that the ultrasonic results can only provide C_0 for $T > 130\,°C$. When the temperature decreases towards T_g, the structural relaxation time becomes so long that even low-frequency ultrasonic measurements detect C_∞ rather than C_0. Lacking any experimental data for the low-temperature C_0, we assumed that the high-temperature C_0 can be linearly extrapolated to lower temperatures.

In agreement with a previous Brillouin-scattering study of CKN by Torell [31], ω_B shows a continuous decrease with increasing temperature and finally joins with ω_0 at high temperatures. γ_B shows a maximum at $T \simeq 230\,°C$ (as also found in [31]) which coincides with the temperature at which the α peak of the depolarized light-scattering $\chi''(\omega)$ curve moves through the frequency of the LA Brillouin peak. This coincidence provides support for the empirical model discussed in the previous section.

IV. DATA ANALYSIS

While early Brillouin-scattering studies of the liquid-glass transition were usually limited to determining the Brillouin frequency and linewidth as functions of temperature, recent experiments have employed data analyses in which the full spectral shape is fit to a theoretical function [34, 22, 35, 23, 6, 36, 11, 13]. However, whether the physical parameters obtained from these analyses are re-

TABLE I. Values of ω_B, γ_B, τ, C_∞, and $f(T)$ obtained from experimental data and analyses.

			CD model				Empirical model	
			$\beta = 0.40$		$\beta = 0.55$			
T (°C)	ω_B (GHz)	γ_B (GHz)	τ (ns)	C_∞ (m/s)	τ (ns)	C_∞ (m/s)	C_∞ (m/s)	$f(T)$
341	10.32	2.29	4.57×10^{-4}	3511	9.84×10^{-4}	3100		
300	10.85	3.11	1.14×10^{-3}	3043	2.41×10^{-3}	2741	2726	0.583
285	11.17	3.37	1.35×10^{-3}	2941	2.86×10^{-3}	2659		
264	11.73	3.81	2.24×10^{-3}	2882	4.61×10^{-3}	2628		
257	11.98	3.98	2.83×10^{-3}	2839	5.72×10^{-3}	2660		
235	12.79	4.06	3.94×10^{-3}	2847	7.69×10^{-3}	2620		
228	13.01	4.03	4.80×10^{-3}	2866	9.14×10^{-3}	2642		
216	13.54	3.82	6.63×10^{-3}	2880	1.21×10^{-2}	2666		
211	13.67	3.70	7.52×10^{-3}	2831	1.33×10^{-2}	2634		
199	14.17	3.43	1.07×10^{-2}	2871	1.80×10^{-2}	2679	2738	0.546
180	14.98	2.83	2.05×10^{-2}	2891	3.13×10^{-2}	2721	2728	0.535
174	15.20	2.65	2.79×10^{-2}	2892	4.08×10^{-2}	2733	2743	0.538
163	15.67	2.34	4.76×10^{-2}	2907	6.29×10^{-2}	2766	2765	0.540
153	16.14	2.00	8.68×10^{-2}	2934	9.99×10^{-2}	2811	2791	0.545
146	16.45	1.79	1.38×10^{-1}	2951	1.44×10^{-1}	2839		
140	16.67	1.66	1.90×10^{-1}	2961	1.78×10^{-1}	2859	2824	0.551
133	17.05	1.45	4.23×10^{-1}	2979	3.25×10^{-1}	2894	2801	0.540
125	17.39	1.20	8.03×10^{-1}	3003	4.92×10^{-1}	2931		
122	17.52	1.14	1.23	3009	6.88×10^{-1}	2943	2846	0.551
117	17.74	1.05	2.35	3022	1.10	2966		
112	17.99	0.91	3.52	3049	1.44	2998	2853	0.549
106	18.17	0.85	4.79	3066	1.73	3019		
100	18.46	0.75	8.35	3105	2.42	3063	2943	0.571
96	18.64	0.71	9.85	3131	2.61	3092		
91	18.86	0.64	2.98×10^{1}	3143	5.75	3113	3034	0.594
85	19.08	0.55	6.60×10^{1}	3168	9.60	3143		
80	19.30	0.49	1.49×10^{2}	3199	1.63×10^{1}	3179	3135	0.616
74	19.55	0.43	4.10×10^{2}	3216	3.06×10^{1}	3201		
69	19.77	0.39	6.36×10^{2}	3251	3.80×10^{1}	3238	3212	0.630
64	19.86	0.35	2.78×10^{3}	3256	9.69×10^{1}	3247		
59	19.93	0.33	1.95×10^{3}	3258	7.09×10^{1}	3248	3230	0.632
53	19.95	0.34	1.44×10^{3}	3269	5.65×10^{1}	3258		
45	20.02	0.33	2.67×10^{3}	3272	8.74×10^{1}	3263	3247	0.631
35	20.08	0.30	5.46×10^{3}	3277	1.31×10^{2}	3270		
23	20.11	0.29	7.14×10^{3}	3274	1.47×10^{2}	3267	3255	0.626
-8	20.39							
-43	20.61							
-78	20.83							
-118	21.05							
-158	21.18							
-193	21.27	0.24						

liable or not, and whether such fits can really determine the correct form of the memory function remain controversial as discussed above.

In this study, we have carried out analyses of the CKN $I_{\rm LA}(\omega)$ data with $I_{\rm LA}(\omega) = I_0 S(q,\omega)/S(q)$ using the models described in Sec. II. In the analyses, we fixed as many of the parameters as possible in the expression for $S(q,\omega)/S(q)$ of Eq. (2.7) by using published experimental results. Comparison of the results obtained with different models provides a means of evaluating the validity of the models.

A. CD memory-function analysis

In this analysis the corrected $I_{\rm LA}(\omega)$ data were fitted using Eq. (2.7) with the CD model of Eq. (2.10) for the memory function $m(\omega)$. The low-temperature value $\gamma_B = 0.24$ GHz (shown in Fig. 5 and Table I) was used for γ in Eq. (2.7) and was assumed to be temperature independent. The linearly temperature dependent ω_0 (shown in Fig. 5) determined from ultrasonic measurements [29, 32] was used.

The CD memory function Eq. (2.10) has three parameters: Δ, $\tau_{\rm CD}$, and $\beta_{\rm CD}$. In the temperature range 68 to 86 °C, the stretching exponent β in Eq. (2.9) was found to be ~ 0.40 from a correlation spectroscopy experiment [37], whereas for $T > 120$ °C, a depolarized light-scattering study found $\beta \simeq 0.55$ [8]. We used these two β values in two individual analyses in which the corresponding $\beta_{\rm CD}$ values in Eq. (2.10) were computed by using the relations of Ref. [24]. Therefore, the three adjustable parameters left in the fits were I_0, Δ, and $\tau_{\rm CD}$.

Two fits to the $I_{\rm LA}(\omega)$ spectra with $\beta = 0.40$ and 0.55 were carried out in the temperature range 341 to 23 °C. The resulting τ and C_∞ values are listed in Table I. A comparison between the best-fit curves and the experimental spectra is shown in Fig. 6 for four temperatures. In general, the fits with $\beta = 0.40$ (solid curves) are good in the whole temperature range. The fits with $\beta = 0.55$ (dashed curves, which are mostly indistinguishable from the solid curves except close to $\omega = 0$) are not as good as those with $\beta = 0.40$ in the temperature range 190 to 100 °C, but are still satisfactory.

In Fig. 7 we show the temperature dependence of τ obtained from the CD fits with $\beta = 0.40$ (circles) and 0.55 (squares) together with the experimental τ values found from depolarized light scattering (lower solid curve) [8] and correlation spectroscopy (upper solid curve) [37]. For $T > 150$ °C, the τ values obtained from both fits agree with the depolarized-light-scattering result. However, for $T < 140$ °C, the τ values found from the fits are unacceptably small when compared to the correlation spectroscopy results. Note that similar disagreements were found in other Brillouin-scattering analyses which used α-relaxation-only memory functions [6, 11, 13]. This result and the sensitivity of τ to the choice of β indicates the insufficiency of α-relaxation-only memory-function models.

In Fig. 8 we show the temperature dependence of C_∞ obtained from the two CD fits (circles, $\beta = 0.40$; squares, $\beta = 0.55$). C_0 and C_B (solid lines) are taken from Fig. 5.

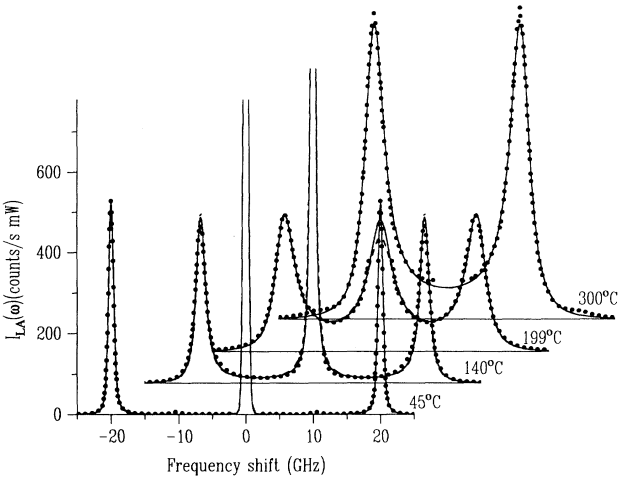

FIG. 6. Best fits to the $I_{\rm LA}(\omega)$ Brillouin spectra (circles) using the CD memory-function model with $\beta_{\rm CD} = 0.264$ ($\beta = 0.40$) (solid lines) and $\beta_{\rm CD} = 0.419$ ($\beta = 0.55$) (dashed lines). (The theoretical spectra for $\beta = 0.40$ and 0.55 are mostly superimposed, except near $\omega = 0$ for $T = 199$ °C.) For clarity, only one-tenth of the points in the experimental spectra are shown in the figure.

As expected, C_∞ joins with C_B at low temperatures. Figure 9 displays the corresponding $f(T)$ obtained from the C_∞ and C_0 values shown in Fig. 8 via Eq. (2.8). Ignoring the high-temperature points above 260 °C which are far above T_m, $f(T)$ found from both CD fits suggests a possible cusp anomaly. However, the apparent T_c values are

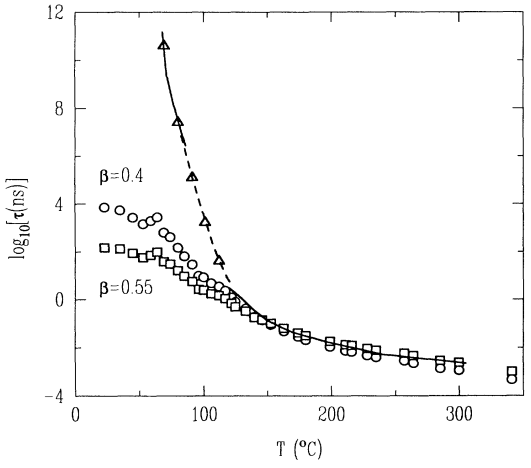

FIG. 7. Temperature dependence of the τ values obtained from the CD memory-function analyses with $\beta = 0.40$ (circles) and 0.55 (squares). The lower and upper solid lines are the experimental τ values from reported depolarized-light-scattering [8] and correlation spectroscopy [37] studies, respectively. The dashed line is just a smooth connection between these two sets of data. The triangles are the values used in Eq. (4.4) for the consistency check of the empirical model for $T < 120$ °C.

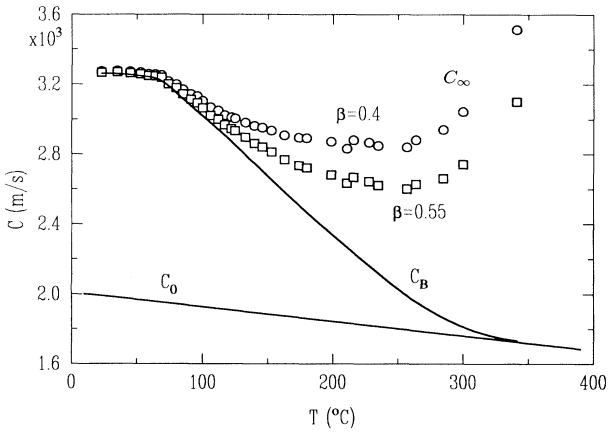

FIG. 8. Temperature dependence of C_∞ obtained from the CD memory-function analyses. The circular and square symbols have the same meaning as in Fig. 7. C_B and C_0 (solid lines) are obtained from Fig. 5.

very different from each other. The fit with $\beta = 0.40$ (circles) suggests $T_c \simeq 120\,^\circ$C, whereas the fit with $\beta = 0.55$ suggests $T_c \simeq 180\,^\circ$C. The T_c values found in this procedure depend strongly on the choice of β, and both values disagree with the T_c ($\sim 100\,^\circ$ C) obtained from previous studies [4, 25, 8].

Besides the two analyses discussed above, we have also carried out CD analyses of the $I_{\rm LA}(\omega)$ data with ω_0 as an additional fitting parameter, and fits of the $I_{\rm VV}(\omega)$ spectra without subtraction of the anisotropic contribution but with an adjustable background added. In the first case, due to the correlation between the parameters Δ, $\tau_{\rm CD}$, and ω_0, the resulting best-fit values changed irregularly with temperature. In the second case, similar to the situation found in Ref. [13], $I_{\rm VV}(\omega)$ could not be fitted well in the temperature range 160 to 300 °C. From these fits, especially the results shown in Figs. 7 and 9, we conclude that although Brillouin-scattering spectra of CKN can be fitted using a CD α-relaxation-only model for the memory function, the resulting parameters are not stable against modification of the model and are not reliable, in agreement with the conclusions of Fuchs, Götze, and Latz [10].

Equation (2.7) shows that the Brillouin-scattering spectrum is determined by the functions $\omega_0^2 - \omega m'(\omega)$ and $\omega m''(\omega)$. In order to illustrate the difference between an α-relaxation-only model and the empirical model we will discuss below, in Fig. 10 we show the predictions of the CD model of Eq. (2.10) with $\beta_{\rm CD} = 0.264$ ($\beta = 0.4$) for these functions. The CD parameters were taken directly from the fits summarized in Table I. Note that as τ increases with decreasing T, the step in $\omega_0^2 - \omega m'(\omega)$ centered around $\omega_0\tau = 1$ moves to the left, causing the Brillouin shift to increase from ω_0 to $\omega_\infty = \sqrt{\omega_0^2 + \Delta^2}$, while the peak in $\omega m''(\omega)$ passes through the position of the Brillouin line producing a linewidth maximum at $\omega_0\tau \simeq 1$ at $T \sim 230\,^\circ$C. The limited frequency range (1.6 to 25 GHz) accessible to the Brillouin-scattering measurement, indicated by the horizontal bars, illustrates the

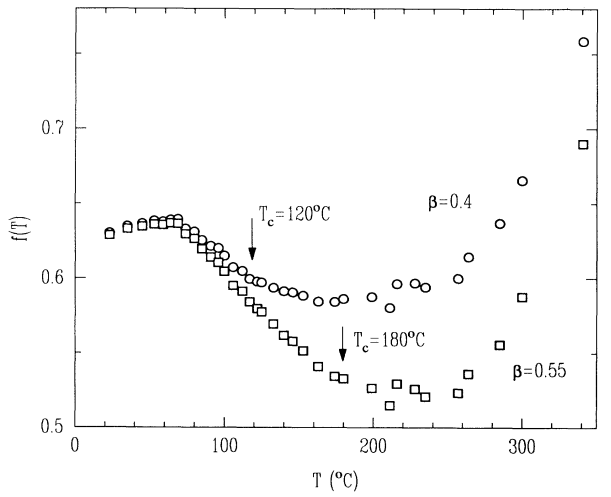

FIG. 9. Temperature dependence of $f(T)$ obtained by using the relation of Eq. (2.8) and the C_∞ and C_0 values shown in Fig. 8. A possible $T_c \simeq 120\,^\circ$C is indicated for the CD analysis with $\beta = 0.40$ (circles), while $T_c \simeq 180\,^\circ$C is found for $\beta = 0.55$ (squares).

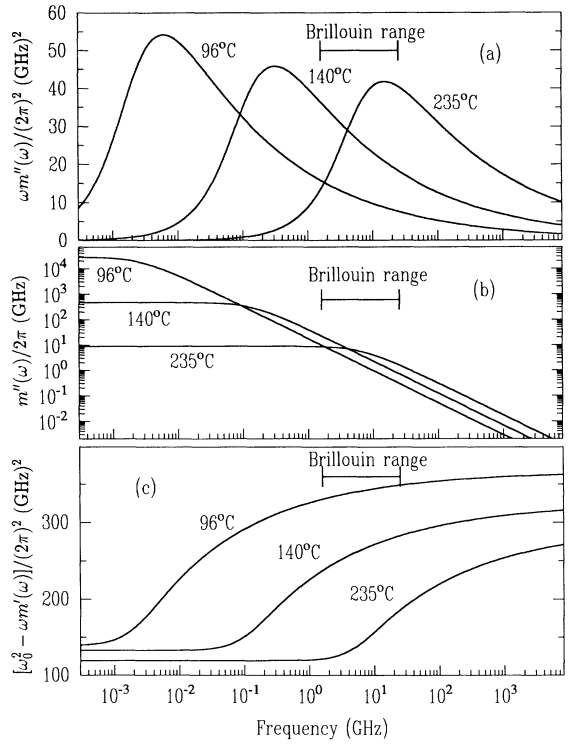

FIG. 10. Predictions of the CD model [Eq. (2.10)] for (a) $\omega m''(\omega)$, (b) $m''(\omega)$, and (c) $\omega_0^2 - \omega m'(\omega)$, with $\beta_{\rm CD} = 0.264$ ($\beta = 0.40$) and $\tau_{\rm CD}$ and C_∞ values obtained from the CD model analysis (Table I). The frequency range of the Brillouin spectra (1.6–20 GHz) is indicated by a horizontal bar. This figure can be compared directly with the results of the empirical model analysis in Fig. 11.

difficulty in establishing the validity of the CD model for the relaxation function.

B. Empirical memory-function analysis

Since the analysis described above shows that α-relaxation-only models for the memory function $m(\omega)$ are inadequate for CKN, we next tried to exploit the depolarized-light-scattering data of Ref. [8] shown in Fig. 2 to construct a complete empirical memory function for CKN as described in Sec. II C 3.

The depolarized-light-scattering spectra determine $R'(\omega)$, so that $m''(\omega)$ will be completely determined by the data of Fig. 2 (apart from a multiplicative constant) in the full range of the Brillouin spectra. To find $m'(\omega)$, we performed the KK transformation [Eq. (2.15)]. For comparison, note that the α-relaxation-only model shown in Fig. 10(a) exhibits only an α peak in the whole frequency range whereas the experimental $\chi''(\omega)$ spectra shown in Fig. 2 contain not only the α peak at low frequency, but also the intermediate β-relaxation structure (and the microscopic peak) which is not contained in the α-relaxation-only model.

In order to compute $m'(\omega)$ for the Brillouin spectral range (1.6 to 25 GHz) with the KK transform, it is necessary to extend $m''(\omega)$ on the low-frequency side to $\omega = 0$. For $T \geq 120\,^{\circ}\mathrm{C}$, since the major part of the α peaks are included in the experimental spectra, we extend the spectra to low frequencies by using the Fourier transform of the Kohlrausch function [Eq. (2.9)] which we fit to the α peaks. The extended $\omega m''(\omega)/BT$ and $m''(\omega)/B$ spectra obtained with this procedure are shown in Figs. 11(a) and 11(b), respectively. For the high-temperature spectra extended this way (305 to 120 °C), the KK transformation procedure gave $m'(\omega)/B$ spectra from which the $-\omega m'(\omega)/BT$ spectra shown in Fig. 11(c) were then computed. [The small "glitches" in the spectra of Figs. 11(c) and 11(d) result from the weak leakage of LA Brillouin components in the original intensity spectra. Although they could have been removed, their presence did not appreciably affect the results of the fits.]

For $T < 120\,^{\circ}\mathrm{C}$, the α peaks have moved below the lower edge of the spectral window at $\omega_L = 0.3$ GHz, so a different strategy is required to complete the KK

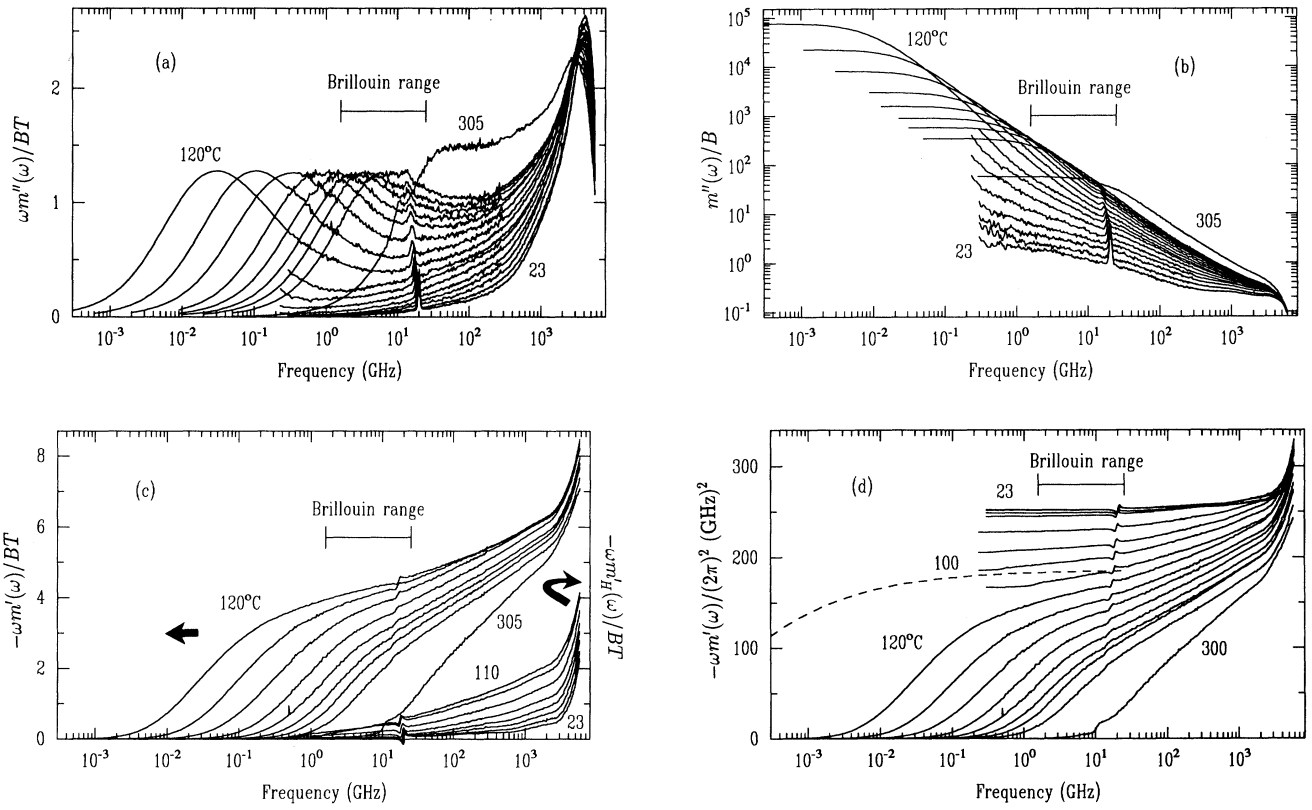

FIG. 11. (a) $\chi''(\omega) = \omega m''(\omega)/BT$ susceptibility spectra obtained from the depolarized-light-scattering spectra of Ref. [8]. The spectra for $T > 120\,^{\circ}\mathrm{C}$ were extended below 0.3 GHz by Fourier transformation of a Kohlrausch function Eq. (2.9) with the β and τ values from Ref. [8]. The temperatures are (from top to bottom) 305, 195, 180 to 60 (with 10 °C per step), 45, and 23 °C. (b) The corresponding $m''(\omega)/B$ spectra. (c) The $-\omega m'(\omega)/BT$ spectra for $T \geq 120\,^{\circ}\mathrm{C}$ and $-\omega m'_H/BT$ spectra for $T < 120\,^{\circ}\mathrm{C}$ obtained by KK transformation of the $m''(\omega)/B$ spectra shown in (b). (d) The $-\omega m'(\omega)$ spectra (solid curves) obtained from the empirical-model analysis. The dashed curve is a plot of $\Delta^2\omega\,\mathrm{Im}(\mathcal{F}\{\exp[-(t/\tau)^{\beta}]\})$ with $\beta = 0.40$ and $\tau = 1.66$ ns, approximating $-\omega m'_\alpha(\omega)$ at $T = 100\,^{\circ}\mathrm{C}$.

transformation procedure.

We note that Eq. (2.15) can be rewritten as

$$m'(\omega) = \frac{2\omega}{\pi}\int_0^{\omega_L} \frac{m''(\omega)-m''(x)}{\omega^2-x^2}dx + \frac{2\omega}{\pi}\int_{\omega_L}^{\infty} \frac{m''(\omega)-m''(x)}{\omega^2-x^2}dx = m'_L(\omega)+m'_H(\omega). \quad (4.1)$$

For ω in the Brillouin range (1.6 to 25 GHz), the second term $m'_H(\omega)$ in Eq. (4.1) can be computed directly; the result is shown in Fig. 11(c) at the lower right. The first term $m'_L(\omega)$ in Eq. (4.1) can be simplified by noting that for ω in the Brillouin range, $x^2 < 0.04\omega^2$ so x^2 can be neglected in the integral; also for $T < 120\,^\circ$C $m''(x) \gg m''(\omega)$ so that $m''(\omega)$ can also be neglected, whence:

$$\omega m'_L(\omega) \approx -(2/\pi)\int_0^{\omega_L} m''(x)dx. \quad (4.2)$$

Therefore, the missing part of the spectrum below $\omega_L = 0.3$ GHz contributes a frequency-independent constant to $-\omega m'(\omega)$ which we will designate as Δ^2, and will treat as an additional fitting parameter. Since Eq. (4.2) is just the integrated area of the α peak, we can equivalently designate m'_L as m'_α and write

$$-\omega m'_\alpha(\omega) = \Delta^2 . \quad (4.3)$$

To illustrate the validity of this result, in Fig. 11(d) we show a plot of $\omega\Delta^2\mathrm{Im}(\mathcal{F}\{\exp[-(t/\tau)^\beta]\})$ (dashed curve, where $\mathcal{F}$ stands for Fourier transformation) with $\beta = 0.40$ (from Ref. [37]) and $\tau = 1.66\times10^3$ ns (extrapolated from Refs. [8] and [37] as shown by the triangular point at $T = 100\,^\circ$C in Fig. 7). The curve approximately represents $-\omega m'_L(\omega)$ at $T \simeq 100\,^\circ$C. The plot indicates clearly that $-\omega m'_L(\omega)$ has reached a constant plateau level in the Brillouin-frequency range. In Fig. 11(d), the full $-\omega m'(\omega)$ curves are shown in which the constant level $-\omega m'_L(\omega) = \Delta^2$ obtained from the fits for $T < 120\,^\circ$C has been added to the $-\omega m'_H(\omega)$ curves shown in Fig. 11(c).

We analyzed the corrected $I_{\mathrm{LA}}(\omega)$ spectra again using Eq. (2.7), but with the empirical memory function of Fig. 11 for $\omega m'(\omega)$ and $\omega m''(\omega)$. The same γ and ω_0 values were used as in the CD model analysis. For $T > 120\,^\circ$C there were only two fitting parameters in the analysis, I_0 and B, while for $T < 120\,^\circ$C there were three: I_0, B, and Δ. Figure 12 shows the best fit to the spectra obtained with this procedure for four temperatures. The analysis produced good fits to the $I_{\mathrm{LA}}(\omega)$ spectra in the full temperature range studied.

C. Determination of C_∞ and $f(T)$

Having shown that the empirical memory function $m(\omega)$ deduced from the depolarized-light-scattering spectra produces fits to the Brillouin-scattering data of at least equal quality to the CD model, we now turn to its implications for C_∞ and $f(T)$.

Comparing Figs. 10(c) and 11(d), we note that while in the CD model $\omega_0^2 - \omega m'(\omega)$ saturates at $\omega_0^2+\Delta^2$ at high frequencies which determines $\omega_\infty^2 = \omega_0^2+\Delta^2$, the empirical model result for $-\omega m'(\omega)$ in Fig. 11(d) increases continuously with increasing ω because of the β relaxation contribution. We can, however, determine the component of $-\omega m'(\omega)$ due to α relaxation alone in order to find an equivalent ω_∞^2 required to evaluate $f(T)$ via Eq. (2.8). For $T \geq 120\,^\circ$C where the α peak has been fit to a stretched exponential [Eq. (2.9)], the Laplace transform of this $m_\alpha(t)$ gives $m'_\alpha(\omega)$, and $\lim_{\omega\to\infty}[\omega m'_\alpha(\omega)] = \Delta^2$ so that $\omega_\infty^2 = \omega_0^2+\Delta^2$. Similarly, for $T < 120\,^\circ$C, the constant Δ^2 in Eq. (4.3) determined from the fits, which is due to the α peak, again fixes $\omega_\infty^2 = \omega_0^2+\Delta^2$.

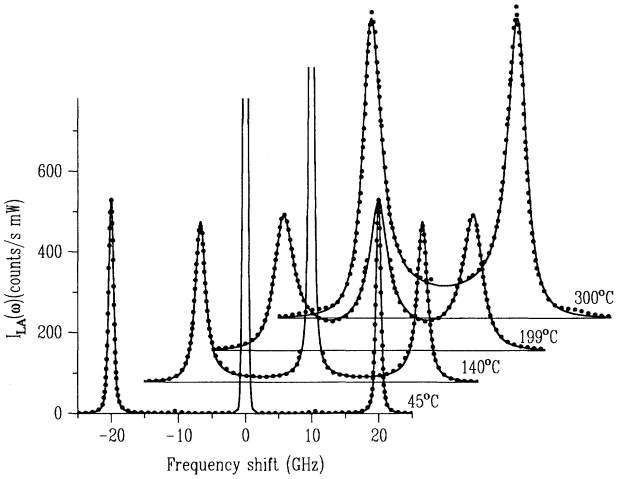

FIG. 12. Best fits (solid curves) to the $I_{\mathrm{LA}}(\omega)$ Brillouin spectra (circles) otained with the empirical model.

The C_∞ values resulting from this analysis are listed in Table I and shown in Fig. 13 (circles). Note that the full value of the $-\omega m'(\omega)$ at the position of the Brillouin peaks will be larger than this plateau value at low temperatures so that ω_B may be larger than ω_∞. In Fig. 13 this $\omega_B > \omega_\infty$ result is seen to occur for a range of temperatures near 100 °C.

Although there is a change of procedure in the analysis of the Brillouin data for $T < 120\,^\circ$C in which an additional fitting parameter Δ is introduced, the consistency of the result is confirmed by the continuity of the resulting C_∞ values around 120 °C.

To further check the consistency of the analysis, we carried out another analysis for $T < 120\,^\circ$C in which we replaced the constant approximation of Eq. (4.2) with

$$\omega m'_L(\omega) = -\Delta^2\omega\,\mathrm{Im}(\mathcal{F}\{\exp[-(t/\tau)^\beta]\}) , \quad (4.4)$$

with $\beta = 0.40$ [37] (and 0.55 [8]) and with the τ values extrapolated from Refs. [8, 37] (triangular points in Fig. 7). The analysis provided fits to the $I_{\mathrm{LA}}(\omega)$ data which were as good as the constant approximation of Eq. (4.2), and the resulting C_∞ values were essentially the same as those obtained by using Eq. (4.2). This result confirms the appropriateness of the approximation of Eq. (4.2) which is β and τ independent. Therefore, we conclude that as long as the contribution of the β relaxation

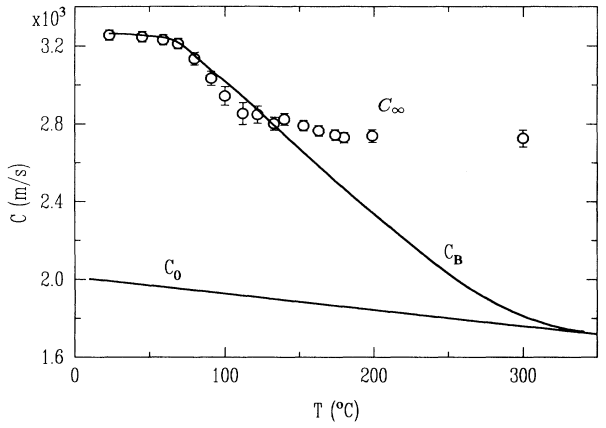

FIG. 13. Temperature dependence of C_∞ (circles) obtained from the empirical-model analysis. C_0 and C_B are the same as Fig. 8.

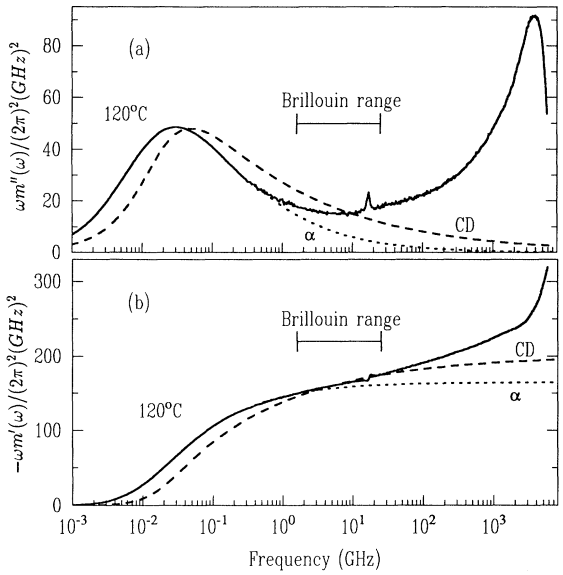

FIG. 14. Comparison of $\omega m''(\omega)$ (a) and $-\omega m'(\omega)$ (b) at $T = 120\,^\circ$C for the CD model (dashed line) and the empirical model (solid line). The dotted curves are the extension of the fit to the α peak using the Kohlrausch function as described in the text.

is taken into account, the analysis will provide a stable result for C_∞.

From this empirical-model analysis, we now also understand the reason that α-relaxation-only models sometimes yield unreasonably small-τ values for low temperatures as shown in Fig. 7. From Fig. 11(a) one can see that even for $T \sim T_g$, where the α peak has completely shifted below 0.3 GHz, $\omega m''(\omega)$ still has a non-negligible value in the normal Brillouin range due to the β relaxation. In fits with the α-relaxation-only model [see Fig. 10(a)], in order to obtain the same level for $\omega m''_\alpha(\omega)$ in this range, the τ value has to be greatly reduced, that is, the α peak has to be artificially shifted to considerably higher frequency so that the high-frequency wing of the α relaxation will appear to provide the contribution of the missing β relaxation. This artificial reduction of τ increases if the α-peak tail of the chosen model is smaller, which explains why the fitted τ obtained with $\beta = 0.55$ is smaller than the one obtained with $\beta = 0.40$. However, this shift of the α peak has essentially no effect on the value of $-\omega m'(\omega)$ in the Brillouin range because it has already reached the plateau value. Therefore, good fits can still be achieved even though the resulting τ values are unphysically small. For temperatures near T_c, the contribution of the β relaxation not only affects the τ value obtained from the α-relaxation-only model, but also the $-\omega m'(\omega)$ values, which will lead to unreliable C_∞ values if β relaxation is ignored.

These effects are illustrated in Fig. 14 where we show $\omega m''(\omega)$ and $-\omega m'(\omega)$ for $T = 120\,^\circ$C obtained from the CD model and empirical model analyses. Note that the α peak of the CD result in (a) is shifted to higher frequencies so that the value of $\omega m''(\omega)$ at the frequency of the Brillouin peak is close to the value of the empirical function. We also show the α contribution (dotted line) resulting from the Kohlrausch fits to the empirical α peak. Note that while the α contribution and the CD fit result in (b) are similar near the Brillioun-peak frequency, the high-frequency limit of the CD function is too large, resulting in an overestimation of C_∞. Therefore, the inclusion of β relaxation clearly plays an important role in the data analysis for CKN and must be included in order to obtain reliable results.

In Fig. 15, we display the temperature dependence of the nonergodicity parameter $f(T)$ (circles) obtained by using the definition of Eq. (2.8) with the C_∞ and C_0 values shown in Fig. 13. [The $f(T)$ values are also listed in Table I.] The data display a cusp anomally as predicted by MCT. The best fit of the $f(T)$ data to the predicted temperature dependence of Eq. (2.4) gave $T_c = 102 \pm 5\,^\circ$C, in good agreement with the T_c values found from

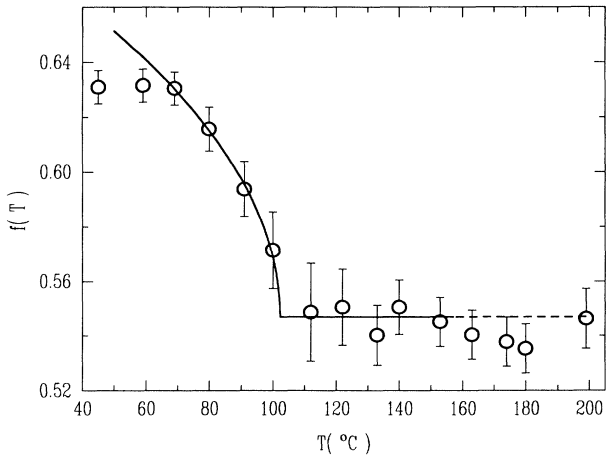

FIG. 15. Temperature dependence of $f(T)$ (circles) obtained from the empirical-model analysis. The best fit (solid line) to Eq. (2.4) yields $f^c \simeq 0.547$ and $T_c \simeq 102.3\,^\circ$C.

neutron-scattering [4] and depolarized light-scattering [8] studies. Also, the $f(T)$ data shown in Fig. 15 closely resemble the results presented in Ref. [10].

V. DIRECT DETERMINATION OF $f(T)$

We have also attempted an alternative approach to the determination of $f(T)$ in the small-q regime probed by Brillouin scattering which does not involve Eq. (2.8) and therefore does not require a determination of C_∞. In analogy with the neutron-scattering approach, one could, in principle, measure the fraction of the scattered intensity within a narrow energy window centered at $\omega = 0$ and thus determine $f(T)$ directly. In practice, however, there are two serious problems with this approach. First, it is extremely difficult to avoid parasitic elastic scattering which adds an uncontrollable signal at $\omega = 0$; second, because the Brillouin peak [which *is* the microscopic peak in the $I_{\rm LA}(\omega)$ spectrum] overlaps the frequency range of the α spectrum when the α peak broadens with increasing temperature (when $T \gtrsim 120\,^\circ$C for CKN), the frequency window set to exclude the Brillouin lines at low temperatures will not be wide enough to contain the whole α peak at high temperatures. Finally, the anisotropic contributions of second-order and rotational scattering must be removed.

The first problem may be avoided by reversing the usual procedure, excluding the signal inside of the selected window around $\omega = 0$ and measuring the integrated signal outside the window. For low temperatures, when the α peak is well separated from the Brillouin peaks, Eq. (2.7) can be approximated as

$$S(q,\omega)/S(q) \cong [S_\alpha(\omega) + S_B(\omega)]/S(q) \ , \qquad (5.1)$$

where $S_\alpha(\omega)$ and $S_B(\omega)$ represent the spectra of the α and Brillouin components. Since the integrated Brillouin intensity is $I_B(T) \propto \int S_B(\omega)d\omega$ while $f(T) = \int S_\alpha(\omega)d\omega/S(q)$ and $S(q) \propto T$, Eq. (5.1) yields

$$f(T) = 1 - AI_B(T)/T \ , \qquad (5.2)$$

where A is a temperature-independent constant. Therefore, by measuring $I_B(T)$, one may determine $f(T)$ directly (up to the unknown constant A) by using Eq. (5.2).

Figure 16 illustrates the separation procedure of Eq. (5.1) where the selected window (0 to 3.3 GHz) is indicated by the line at 3.3 GHz which corresponds approximately to the minimum of $\omega I_{\rm LA}(\omega)$ at 134 °C. The $I_{\rm LA}$ spectrum was obtained by subtracting the background and depolarized-scattering contribution from a VV spectrum following the procedure discussed in Sec. III. The resulting $f(T)$, computed via Eq. (5.2) from the integrated intensity outside of the window, is shown by the solid circles in Fig. 17. Although the anticipated decrease of $f(T)$ with increasing temperature is observed on approaching T_c, $f(T)$ continues to decrease with increasing T above T_c rather than exhibiting a cusp. This is a consequence of the broadening of the α peak so that an increasing part of its total intensity falls outside of the selected 3.3 GHz window as T increases. We note that in the neutron-scattering study of polybutadiene by Frick, Farago, and Richter, a similar result was obtained before invoking a special correction procedure (see Fig. 3 of Ref. [5]).

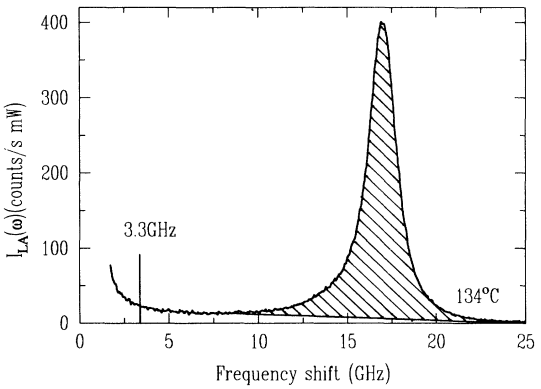

FIG. 16. $I_{\rm LA}(\omega)$ spectrum at $T = 134\,^\circ$C illustrating the separation of Eq. 5.1. The shaded area represents I_B; the line at 3.3 GHz indicates the selected window.

Although the separation indicated by Eq. (5.1) becomes ambiguous once the α peak broadens sufficiently to overlap the Brillouin peaks, we attempted an *ad hoc* separation of the two parts of $S(q,\omega)$ by drawing a baseline under the Brillouin component and determining the integrated area indicated by the shaded region in Fig. 16. This area was taken to be $I_B(T)$ in Eq. (5.2). The constant A was arbitrarily fixed to make $f(T = 70\,^\circ\text{C}) = 0.65$, to agree with the result of the analysis of Sec. IV B. The resulting $f(T)$ values are shown in Fig. 17 by open symbols; the five different symbols represent five

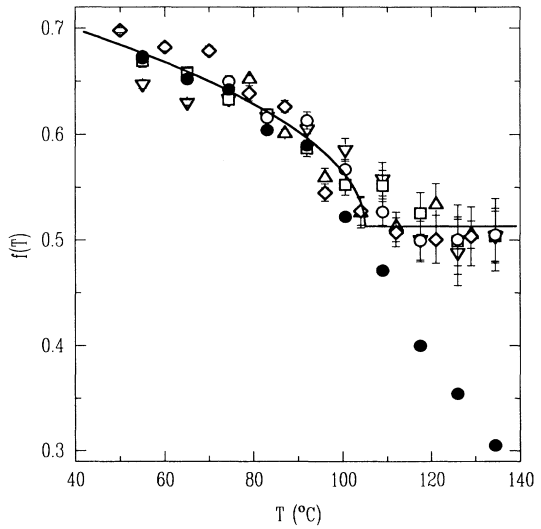

FIG. 17. $f(T)$ deduced from Eq. (5.2). The solid circles are the result of integrating the intensity between 3.3 and 25 GHz. The open symbols are the result of Eq. (5.2) where I_B is the area of the shaded region in Fig. 15. The five different symbols represent five separate sets of experiments. The solid curve is the fit to Eq. (2.4).

different sets of experiments. This procedure resulted in a weak cusp in $f(T)$ at $T \sim 105\,^{\circ}\mathrm{C}$, in agreement with the other determinations of T_c.

As noted by Götze [14], since the dynamic part of S_q is proportional to T/C_0^2, the coefficient A in Eq. (5.2) is more accurately given by $A \propto 1/C_0^2$. We have reanalyzed the data shown in Fig. 17 using the C_0 values shown in Fig. 8. The result is essentially unchanged, except that the constant level of $f(T)$ above T_c is slightly higher, closer to the result shown in Fig. 15.

VI. SUMMARY AND CONCLUSIONS

A Brillouin-scattering study of CKN was carried out in order to test the MCT prediction of the q independence of T_c. The anisotropic and background contributions were subtracted in order to obtain pure LA-mode Brillouin spectra for the analysis.

An analysis employing a conventional Cole-Davidson memory function produced good fits to the spectra as found in previous publications. However, the relaxation times resulting from the fits do not increase sufficiently fast as T decreases towards T_g. Furthermore, while fits of equal quality can be found with different values of the stretching exponent β, the form of $f(T)$ and the resulting value of T_c were found to depend strongly on the β used in the analysis. We therefore concluded that while Cole-Davidson or stretched-exponential α-relaxation-only models can provide good fits to the spectra, the parameters τ and C_∞ produced by the fits are not meaningful due to the neglect of β-relaxation effects, and the fits cannot reliably locate T_c.

A second analysis was therefore carried out in which an empirical memory function was constructed, starting from previously reported depolarized-light-scattering spectra, which includes both α and β relaxation. Although this approach was motivated by the insights of MCT, the construction of the memory function does not depend on any MCT results. This analysis revealed the origin of the inadequacy of α-relaxation-only models and demonstrated the importance of including β relaxation in the analysis. By extrapolating the α-relaxation contribution to the memory function and determining C_∞ which only corresponds to the α relaxation, the analysis produced a nonergodicity parameter $f(T)$ which exhibits a cusp anomaly as predicted by MCT at $T_c \sim 102\,^{\circ}\mathrm{C}$, in good agreement with the T_c values obtained from neutron-scattering [4] and depolarized-light-scattering [8] studies. This result demonstrates that for CKN there is no contradiction between the small-q results of normal Brillouin scattering (i.e., the $q \to 0$ limit) and the neutron- ($q \sim q_0$) or depolarized-light-scattering results, in agreement with the MCT.

It is important to note that the α- and β-relaxation processes in supercooled liquids are stretched, and a large frequency window is required to accurately reveal their structure. Normal Brillouin scattering covers a spectral range of just over one decade and is not able to determine the structure of the relaxation dynamics unambiguously. As we have discussed here and in Ref. [23], and as Montrose, Solovyev, and Litovitz [21] and Fuchs, Götze, and Latz [10] have also noted, Brillouin-scattering data can be fit quite accurately with α-relaxation-only models, even with quite different values of the streteching parameter β. However, the results of such fits are not likely to be physically meaningful once the temperature is low enough that the β relaxation enters the experimental frequency window. Only when a *complete* memory function is used can the analysis of Brillouin-scattering data provide reliable and meaningful results, particularly for τ and C_∞, and this requires that the memory function be independently determined.

We also suggest that the results of the present investigation may have implications of much greater generality than the controversy concerning the question of identifying T_c in $S(q,\omega)$ for different values of q which motivated our study. For many years the results of experimental studies of supercooled liquids have been analyzed with stretched-exponential or Cole-Davidson models. Our results suggest that the relaxation times found in such analyses may have been affected by the neglect of β-relaxation processes whenever the frequency of the experimental probe was above the α-relaxation peak.

Finally, we note that the somewhat arbitrary procedures we have used in extending $m''(\omega)$ to lower frequencies might be avoided by extending the measurements to lower frequencies or combining our depolarized-light-scattering data with photon correlation, ultrasonic, dielectric, or other experimentally determined $m''(\omega)$ data. The feasibility of this approach is currently under study.

ACKNOWLEDGMENTS

We are deeply indebted to W. Götze for numerous helpful discussions and suggestions during the course of this work. We thank M. Fuchs for providing Fig. 1. We also thank I. Halalay, C. Dreyfus, R. Pick, C.A. Angell, L. Torell, S. Nagel, L. Börjesson, and M. Elmroth for helpful conversations. This research was supported by the U.S. National Science Foundation under Grant No. DMR-9014344.

[1] W. Götze, in *Liquids, Freezing and the Glass Transition*, edited by J.P. Hansen, D. Levesque, and J. Zinn-Justin (North-Holland, Amsterdam, 1991), p. 287.
[2] W. Götze and L. Sjögren, Rep. Prog. Phys. **55**, 241 (1992).
[3] W. Götze, Z. Phys. B **60**, 195 (1985).
[4] F. Mezei, W. Knaak, and B. Farago, Phys. Scr. **19**, 363 (1987).
[5] B. Frick, B. Farago, and D. Richter, Phys. Rev. Lett. **64**, 2921 (1990).
[6] L. Börjesson, M. Elmroth, and L.M. Torell, Chem. Phys. **149**, 209 (1990).

[7] W. Petry, E. Bartsch, F. Fujara, M. Kiebel, H. Sillescu, and B. Farago, Z. Phys. B **83**, 175 (1991).
[8] G. Li, W.M. Du, X.K. Chen, H.Z. Cummins, and N.J. Tao, Phys. Rev. A **45**, 3867 (1992).
[9] G. Li, W.M. Du, A. Sakai, and H.Z. Cummins, Phys. Rev. A **46**, 3343 (1992).
[10] M. Fuchs, W. Götze, and A. Latz, Chem. Phys. **149**, 185 (1990).
[11] M. Elmroth, L. Börjesson, and L.M. Torell, Phys. Rev. Lett. **68**, 79 (1992).
[12] L. Börjesson and W.S. Howells, J. Non-Cryst. Solids **131-133**, 53 (1991).
[13] C. Dreyfus, M.J. Lebon, H.Z. Cummins, J. Toulouse, B. Bonello, and R.M. Pick, Phys. Rev. Lett. **69**, 3666 (1992).
[14] W. Götze (private communication).
[15] U. Bengtzelius, W. Götze, and A. Sjölander, J. Phys. C **17**, 5915 (1984).
[16] L. Sjögren and W. Götze, in *Dynamics of Disordered Materials*, edited by D. Richter, A.J. Dianoux, W. Petry, and J. Teixeira, Springer Proceedings in Physics Vol. 37 (Springer-Verlag, Berlin, 1989), p. 18.
[17] M. Fuchs, W. Götze, S. Hildebrand, and A. Latz, J. Phys. Condens. Matter **4**, 7709 (1992).
[18] H.Z. Cummins, W.M. Du, M. Fuchs, W. Götze, S. Hildebrand, A. Latz, G. Li, and N.J. Tao, Phys. Rev. E **47**, 4223 (1993).
[19] R.D. Mountain, Rev. Mod. Phys. **38**, 205 (1966).
[20] R.D. Mountain, J. Res. Natl. Bur. Stand. Sec. A **70**, 207 (1966); **72**, 95 (1968).
[21] C.J. Montrose, V.A. Solovyev, and T.A. Litovitz, J. Acoust. Soc. Am. **43**, 117 (1968).
[22] N.J. Tao, G. Li, and H.Z. Cummins, Phys. Rev. B **43**, 5815 (1991).
[23] N.J. Tao, G. Li, and H.Z. Cummins, Phys. Rev. B **45**, 686 (1992).
[24] C.P. Lindsey and G.D. Patterson, J. Chem. Phys. **73**, 3348 (1980).
[25] W. Knaak, F. Mezei, and B. Farago, Europhys. Lett. **7**, 529 (1988).
[26] W. Doster, S. Cusack, and W. Petry, Phys. Rev. Lett. **65**, 1080 (1990).
[27] M. Kiebel, E. Bartsch, O. Debus, F. Fujara, W. Petry, and H. Sillescu, Phys. Rev. B **45**, 10 301 (1992).
[28] W. Götze and L. Sjögren, Phys. Rev. A **43**, 5442 (1991).
[29] R. Weiler, R. Bose, and P.B. Macedo, J. Chem. Phys. **53**, 1258 (1970).
[30] K.I. Rao, D.B. Helphrey, and C.A. Angell, Phys. Chem. Glasses **14**, 16 (1973).
[31] L.M. Torell, J. Chem. Phys. **76**, 3467 (1982).
[32] L.T. Cheng, Y.X. Yan, and K.A. Nelson, J. Chem. Phys. **91**, 6052 (1989).
[33] G. Li, N. Tao, L.V. Hong, H.Z. Cummins, C. Dreyfus, M. Hebbache, R.M. Pick, and J. Vagner, Phys. Rev. B **42**, 4406 (1990).
[34] M. Soltswisch, J. Sukmanowski, and D. Quitmann, J. Chem. Phys. **86**, 3207 (1986).
[35] L. Börjesson, M. Elmroth, and L.M. Torell, J. Non-Cryst. Solids **131-133**, 139 (1991).
[36] S. Loheider, G. Vögler, I. Petscherizin, M. Soltwisch, and D. Quitmann, J. Chem. Phys. **93**, 5436 (1990).
[37] D.L. Sidebottom and C.M. Sorensen, J. Chem. Phys. **91**, 7153 (1989).